



Enhanced electrochemical performance of $\text{LiNi}_{0.83}\text{Co}_{0.12}\text{Mn}_{0.05}\text{O}_2$ cathodes with a fast-ion conductor $\text{Li}_{0.33}\text{La}_{0.56}\text{TiO}_3$ coating layer

Yonglin Wu¹ · Hongdi Cui¹ · Xiaojuan Liu¹ · Xiaohui Zhong¹ · Zhifeng Li¹ · Chunxiang Wang¹ · Sydorov Dmytro¹

Received: 9 January 2023 / Revised: 14 February 2023 / Accepted: 3 March 2023 / Published online: 8 March 2023
© The Author(s), under exclusive licence to Springer-Verlag GmbH Germany, part of Springer Nature 2023

Abstract

Ni-rich layered cathode materials $\text{LiNi}_x\text{Co}_y\text{Mn}_{(1-x-y)}\text{O}_2$ ($x \geq 0.8$) suffer from capacity decay due to structural deterioration during electrochemical cycling. To overcome these problems, the fast-ion conductor $\text{Li}_{0.33}\text{La}_{0.56}\text{TiO}_3$ (LLTO) is coated on the surface of $\text{LiNi}_{0.83}\text{Co}_{0.12}\text{Mn}_{0.05}\text{O}_2$ (NCM83) cathodes through the sol–gel method, which can stabilize the electrode/electrolyte interface of cathode materials and facilitate Li^+ transport and charge transfer. As a result, the LLTO-coated NCM83 exhibits better cycle stability and higher rate performance. The NCM83 modified by 5 wt% LLTO has the discharge capacity of 185.9 mAh g^{-1} at 1C rate after 100 cycles and with higher capacity retention of 92.9% than the pristine NCM83 of 86.2%, and as well as the 5 wt% LLTO-coated NCM83 has a higher Li^+ -insert diffusion coefficient of $1.143 \times 10^{-11} \text{ cm}^2 \text{ s}^{-1}$ than the pristine NCM83 of $8.757 \times 10^{-12} \text{ cm}^2 \text{ s}^{-1}$. Therefore, the fast-ion conductor LLTO coating strategy shows great potential in improving the performance of Ni-rich layered cathode materials.

Keywords Lithium ion battery · Cathode materials · $\text{LiNi}_{0.83}\text{Co}_{0.12}\text{Mn}_{0.05}\text{O}_2$ · Surface coating · $\text{Li}_{0.33}\text{La}_{0.56}\text{TiO}_3$

Introduction

High-specific energy lithium-ion batteries (LIBs) have been widely used in electric vehicles. The development of electrode materials with high energy density and enhanced safety is a crucial research focus for LIBs. Among the promising electrode materials, Li-rich layered cathode materials, Ni-rich layered cathode materials, and lithium metal anode materials have drawn significant attention [1–4]. Specifically, Ni-rich layered cathode materials, such as $\text{LiNi}_x\text{Co}_y\text{Mn}_{(1-x-y)}\text{O}_2$ ($x \geq 0.8$, NCM), exhibit high real energy, high operating voltage, and reasonable prices and are considered as the future trend of cathode materials [5, 6]. However, these materials suffer from capacity decay due to structural deterioration during electrochemical cycling [7–10]. Various strategies have been devoted to improving the structural stability of these materials, including

elemental doping [11–13], surface coating [14–16], and structural design [17–19].

Among them, the surface coating can prevent the surface of NCM cathode materials from directly contacting with organic electrolyte, reduce the interface side reaction, and thus improve the cycle stability of the NCM cathodes. The common coating agents mainly include oxides (AlO_3 [20, 21], MgO [22, 23]), phosphates (FePO_4 [24, 25], $\text{Ni}_3(\text{PO}_4)_2$ [26, 27]), and fluorides (CaF_2 [28, 29], AlF_3 [30, 31]). However, these materials have poor ionic and electronic conductivity, which will hinder the migration of ions and electrons and increase the electrochemical polarization and interface impedance. As such, alternative coating materials with excellent lithium ion conductivity, wide electrochemical window, and good thermal stability have been explored.

Lithium-ion-based fast-ion conductors have emerged as effective coating materials in this context. For example, Yan et al. [32] used Li_3PO_4 to coat the $\text{LiNi}_{0.76}\text{Mn}_{0.14}\text{Co}_{0.10}\text{O}_2$ materials by using the atomic layer deposition method, which greatly improved the capacity retention and voltage stability of the materials. Xiao et al. [33] used LiTa_2PO_8 as a coating layer to modify the $\text{LiNi}_{0.8}\text{Mn}_{0.1}\text{Co}_{0.1}\text{O}_2$ cathodes, and the capacity retention increased from 71.58% to 84.85% after 100 cycles. It is pointed out that $\text{Li}_{3x}\text{La}_{2/3-x}\text{TiO}_3$ (LLTO) as fast-ion conductor with higher ion conductivity (up to 10^{-3}

✉ Zhifeng Li
jxlzfeng@163.com

✉ Chunxiang Wang
jwxchx1979@126.com

¹ School of Materials Science and Engineering, Jiangxi Provincial Key Laboratory of Power Batteries and Materials, Jiangxi University of Science and Technology, Ganzhou 341000, People's Republic of China

S·cm⁻¹), making it an excellent candidate as a coating material. Fan et al. [34] used crystalline Li_{0.35}La_{0.55}TiO₃ (LLTO) as a surface coating layer to enhance the structural stability of the single-crystal LiNi_{0.6}Co_{0.2}Mn_{0.2}O₂ (SNCM622) cathode in sulfide-based all-solid-state lithium batteries, the S-NCM622@LLTO cathode exhibit excellent cycling performance with 84.5% capacity retention after 100 cycles at 0.1 C at room temperature. Liu et al. [35] enhanced the electrochemical performance of LiNi_{0.6}Co_{0.2}Mn_{0.2}O₂ by amorphous LLTO surface modification.

In general, Ni-rich layered cathode materials are easy to form lithium residues (such as LiOH, Li₂O) on the material surface during high-temperature synthesis. Then Li₂O react with moisture and CO₂ in the air generating lithium residual compounds such as Li₂CO₃, LiHCO₃, and LiOH. Besides, during the process of cooling and storing, the surface layer of the cathode material is reconstructed, and lithium is removed from the lattice and reacts with H₂O and CO₂ in the air to form lithium residual compounds [36–38]. Lithium residual compounds will accelerate the decomposition of the electrolyte [39], increase the transfer impedance of Li⁺ ions at the electrode/electrolyte interface, and thus deteriorate the electrochemical performance of the cathode material [40]. From above, it shows that lithium residues will be formed during the high-temperature synthesis of Ni-rich cathode materials; therefore, it is inefficient to eliminate the lithium residual by coating fast ion conductors on the surface of such cathode materials.

Here, we propose an ingenious strategy to inhibit the formation of these lithium residues and form a uniform LLTO coating layer on the surface of the LiNi_{0.83}Co_{0.12}Mn_{0.05}O₂ cathode materials. Firstly, LLTO precursor is formed on the surface of Ni_{0.83}Co_{0.12}Mn_{0.05}(OH)₂ precursor by sol–gel method, and then LLTO-coated LiNi_{0.83}Co_{0.12}Mn_{0.05}O₂ is synthesized by one-step high-temperature sintering. This method can make the LiNi_{0.83}Co_{0.12}Mn_{0.05}O₂ cathode materials form close interface contact with the fast ion conductor, as well as inhibit the formation of surface lithium residues, and then the electrochemical properties of LiNi_{0.83}Co_{0.12}Mn_{0.05}O₂ cathode materials are greatly improved.

Experiment

Preparation of pristine-NCM and NCM83-LLTO

The precursor Ni_{0.83}Co_{0.12}Mn_{0.05}(OH)₂ was prepared by the co-precipitation method. The Ni_{0.83}Co_{0.12}Mn_{0.05}(OH)₂ precursor was first mixed with LiOH·H₂O (5 mol% excess) and then calcined at 550 °C for 6 h and at 780 °C for 12 h to obtain LiNi_{0.83}Co_{0.12}Mn_{0.05}O₂ (NCM83).

LLTO-coated NCM83 was prepared as follows: LiOH·H₂O (99.9%, Aladdin), La(NO₃)₃·6H₂O (99.99%, Aladdin), and Ti(C₄H₉O)₄ (99%, Aladdin) were dissolved in anhydrous ethanol in the molar ratio of 0.33:0.56:1 to obtain a mixed solution. An appropriate amount of citric acid was added and stirred for 6 h. Then a certain amount of Ni_{0.83}Co_{0.12}Mn_{0.05}(OH)₂ was added and sonicated for 2 h to make it fully dispersed, followed by stirring in a water bath at 80 °C until the solvent evaporated. The obtained precursors were dried in air at 120 °C for 12 h, mixed with LiOH·H₂O after grinding and crushing, held at 550 °C for 6 h and at 780 °C for 12 h for sintering, and then reduced to room temperature to finally obtain NCM83-LLTO materials. The obtained composites with different amounts of LLTO (3, 5, 7, and 50 wt%) are denoted as NCM83-0.03LLTO, NCM83-0.05LLTO, NCM83-0.07LLTO, and NCM83-0.5LLTO, respectively.

Structure and morphology characterization

The diffraction data of the samples were obtained by X-ray diffractometer (Bruck D8 Advance, Germany) at the scanning angle range of 10° ~ 85° with a scanning rate of 5°·min⁻¹. Field emission scanning electron microscope (SEM) (ZEISS SIGMA300) and transmission electron microscope (TEM) (Tecnai G2-20) were used to study morphology and detailed structure of the obtained samples. The specific surface area of the sample was measured by the Bruner-Emmett-Taylor (BET) method, which was based on a nitrogen adsorption–desorption test performed at 77.3 K with a Micromeritics ASAP 2020 automatic microporous chemical adsorption physical adsorption analyzer. An X-ray photoelectron spectroscopy (XPS) (Thermo Scientific K-Alpha) was used to analyze the chemistry of the sample element's valence.

Electrochemical measurement

The active material, polyvinylidene fluoride (PVDF), and acetylene black (SP) were weighed according to the mass ratio of 8:1:1, and N-methyl-pyrrolidone (NMP) was added as the solvent to make the slurry mixed well. After mixing well, the slurry was evenly coated on the current collector Al foil and then cut into small discs with a radius of 6 mm and dried in a vacuum drying oven at 60 °C for 12 h. The obtained electrode sheet was assembled into CR2032 button batteries using a lithium sheet as the counter electrode, Celgard 2300 type diaphragm as a separator, and 1 mol L⁻¹ LiPF₆ ethylene carbonate/diethyl carbonate (EC/DEC) solution as the electrolyte in a glove box filled with argon. The electrochemical measurements were conducted to test the rate and cycle performance of prepared samples

through the automatically galvanostatical battery test system (NEWARE). The electrochemical impedance measurement was characterized by the CHI660E electrochemical workstation with a frequency of 0.01 Hz–100 kHz. Cyclic voltammetry (CV) was performed on the electrochemical workstation (CHI660E) at voltages ranging from 2.5 to 4.6 V in the scanning rate from 0.1 to 1 mV s^{-1} .

Results and discussion

Structure and morphology analysis

Figure 1a shows the XRD diffraction patterns of Pristine-NCM83 and three different ratios of NCM83-LLTO. The comparison with the standard PDF card of LiNiO_2 (PDF#09–0063) shows that the samples are all hexagonal crystalline $\alpha\text{-NaFeO}_2$ layered structure with a space group of $R\bar{3}m$. From the apparent diffraction peak splitting of the (006)/(102) and (108)/(110) pairs, an ordered layered structure is formed, and the c/a values are higher than 4.9 [41]. In addition, no corresponding LLTO phases are detected in the XRD patterns of the LLTO-coated samples, which may be caused by the low amount of LLTO coating or the formation of amorphous coating layers. To verify this, a sample with an increased coating amount up to 50 wt% is prepared using the same method, and the test results are shown in Fig. 1b, in which the diffraction peaks of (110), (200), and (212) are found to match the LLTO phases (PDF#87–0935).

In order to investigate the effect of LLTO coating on the surface composition and elemental valence of NCM materials, Pristine-NCM and NCM-0.05LLTO are characterized with XPS, and the results are shown in Fig. 2. By comparing

Fig. 2a, c, and d, the binding energies of La $3d_3$, Ti $2p_{3/2}$, and Ti $2p_{1/2}$ can be detected at 853.64 eV, 456.48 eV, and 462.37 eV, respectively [42], which indicating the presence of LLTO coating on the surface of the coated NCM material. In Fig. 2b, after splitting the peaks, the percentages of Ni^{2+} in the Pristine-NCM and NCM-0.05LLTO samples are calculated to be 33.33% and 30.76%, respectively. The decrease in the percentage of Ni^{2+} indicates that the LLTO coating improves the surface stability of the material and reduces the formation of NiO on the surface [43].

Figure 3 shows the SEM images of the samples and the EDS and TEM images of NCM83-0.05LLTO. It is discovered by comparing Fig. 3a–c, and d that all samples are made up of spherical secondary particles with a diameter of 10 nm, and the surface of the material becomes rougher with the amount of LLTO coating increased. In addition, EDS analysis is used to further confirm the uniformity of the LLTO coating. The elemental mapping results corresponding to NCM83-0.05 LLTO in Fig. 3e show that the La and Ti components are uniformly distributed on the material surface. To further investigate the detailed microstructure of LLTO-coated NCM83, TEM tests are performed on NCM83-0.05LLTO as shown in Fig. 3f, and the HRTEM images show two different crystal plane spacings corresponding to the (112) face of LLTO ($d \sim 0.220$ nm) and the (003) face of NCM83 ($d \sim 0.472$ nm) respectively, and it can be clearly found that NCM83 is uniformly covered with a coating of about 2 nm, which is consistent with the test results of XRD and EDS.

The nitrogen adsorption–desorption isotherms and pore size distribution curves of Pristine-NCM83 and NCM83-0.05LLTO after coating treatment are obtained by the Brunauer–Emmett–Teller (BET) method, as shown in Fig. 4a, b, and the isotherms are classified according to IUPAC. The

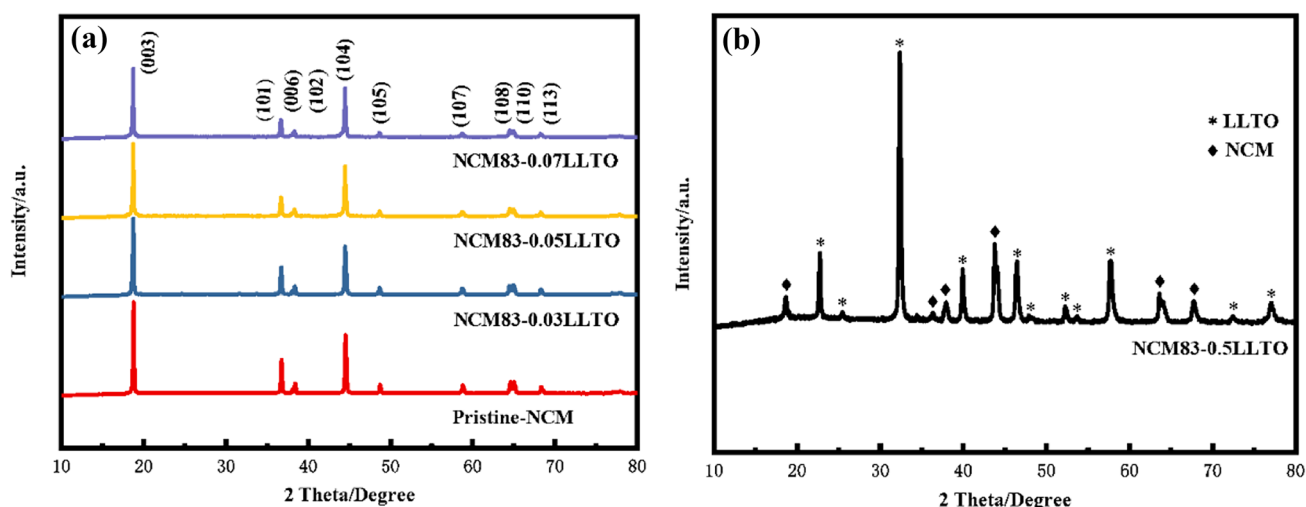


Fig. 1 **a** The XRD diffraction pattern of Pristine-NCM, NCM83-0.03LLTO, NCM83-0.05LLTO, NCM83-0.07LLTO; **b** the XRD diffraction pattern of NCM83-0.5LLTO

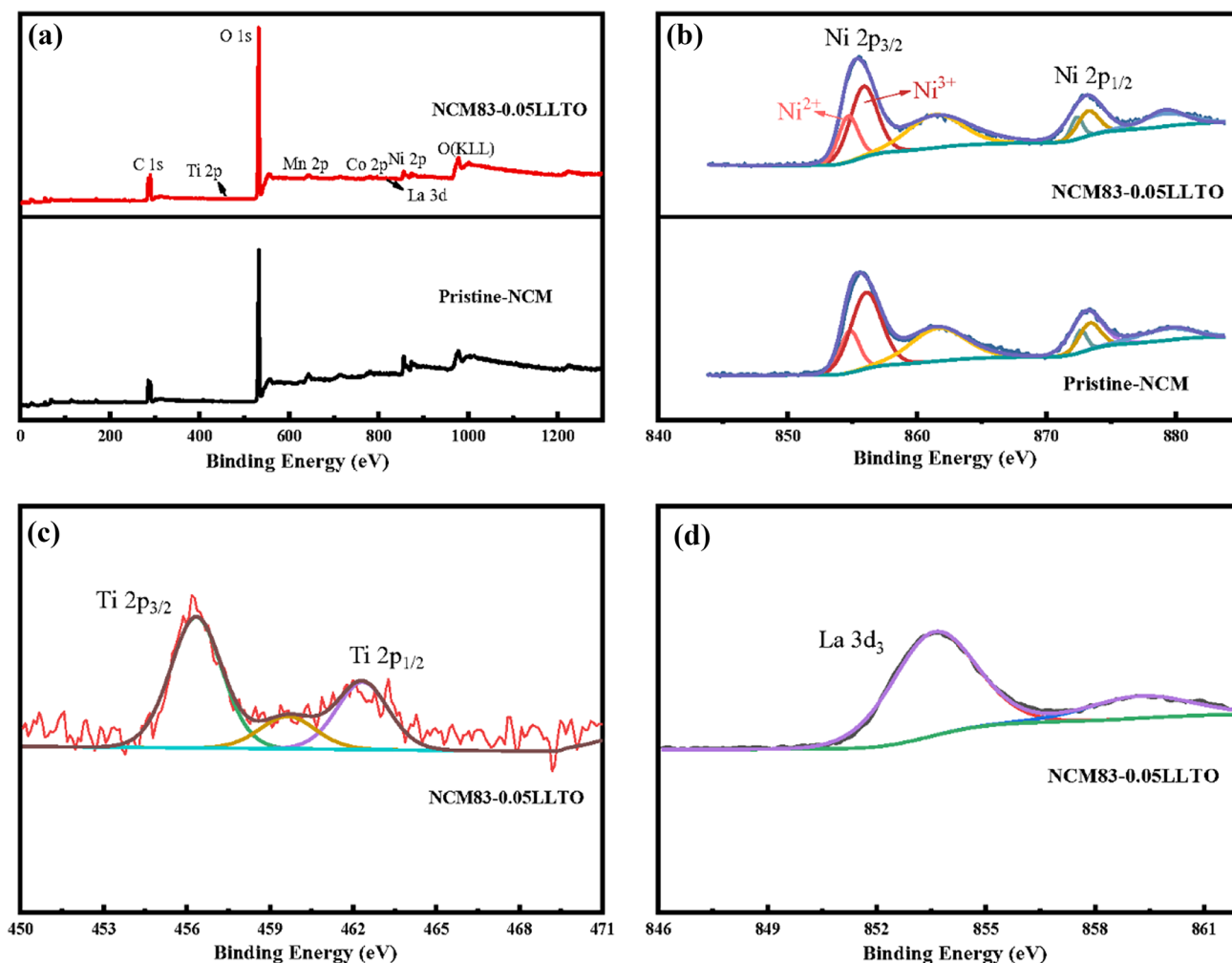


Fig. 2 XPS profiles of Pristine-NCM and NCM83-0.05LLTO samples and the fitting results of individual elemental profiles: **a** XPS full spectrum; **b** Ni2p; **c** Ti2p; **d** La3d

curves are all type III isotherms, and the pore size distribution shows that the material is mostly mesoporous. It is calculated that the specific surface area of NCM83 after coating treatment changed from 1.5923 to 0.9235 m² g⁻¹, and the average pore size changed from 11.8068 to 16.0260 nm. The reduction of the specific surface area of the material after coating implies that the coated LLTO can fill the partial gap of primary particles on the material surface. The reduction in specific surface area can reduce the direct contact between the active material and the electrolyte, thus alleviating the side reactions at the interface.

Analysis of electrochemical performance

Electrochemical tests are performed on pristine NCM83 and LLTO-coated NCM83 to investigate the effect of LLTO coating on the electrochemical performance of NCM83. The initial charge/discharge curves of four samples at 0.1

C current density and 2.8–4.2 V voltage range are shown in Fig. 5a. Compared with the 200.3 mAh g⁻¹ discharge capacity of Pristine-NCM, the discharge capacities of NCM83-0.03LLTO, NCM83-0.05LLTO, and NCM83-0.07LLTO are only 198.0 mAh g⁻¹, 196.3 mAh g⁻¹, and 194.6 mAh g⁻¹, respectively. However, the corresponding coulombic efficiency is 92.06%, 91.24%, and 91.16%, respectively, which was slightly larger than that of Pristine-NCM83 (91.10%). The relatively low discharge capacity of the LLTO-coated NCM83 can be attributed to a decrease in the amount of active material, while the relatively high coulomb efficiency indicates that the protection provided by the LLTO coating can reduce side reactions and irreversible capacity loss during charging and discharging.

The rate performance is evaluated at various current densities from 0.2 to 5 C at 4.3 V. From Fig. 5b, NCM83-0.05 LLTO exhibits good rate performance, which has a discharge capacity of 202.2 mAh g⁻¹ at 0.2 C in the 30th turn. The

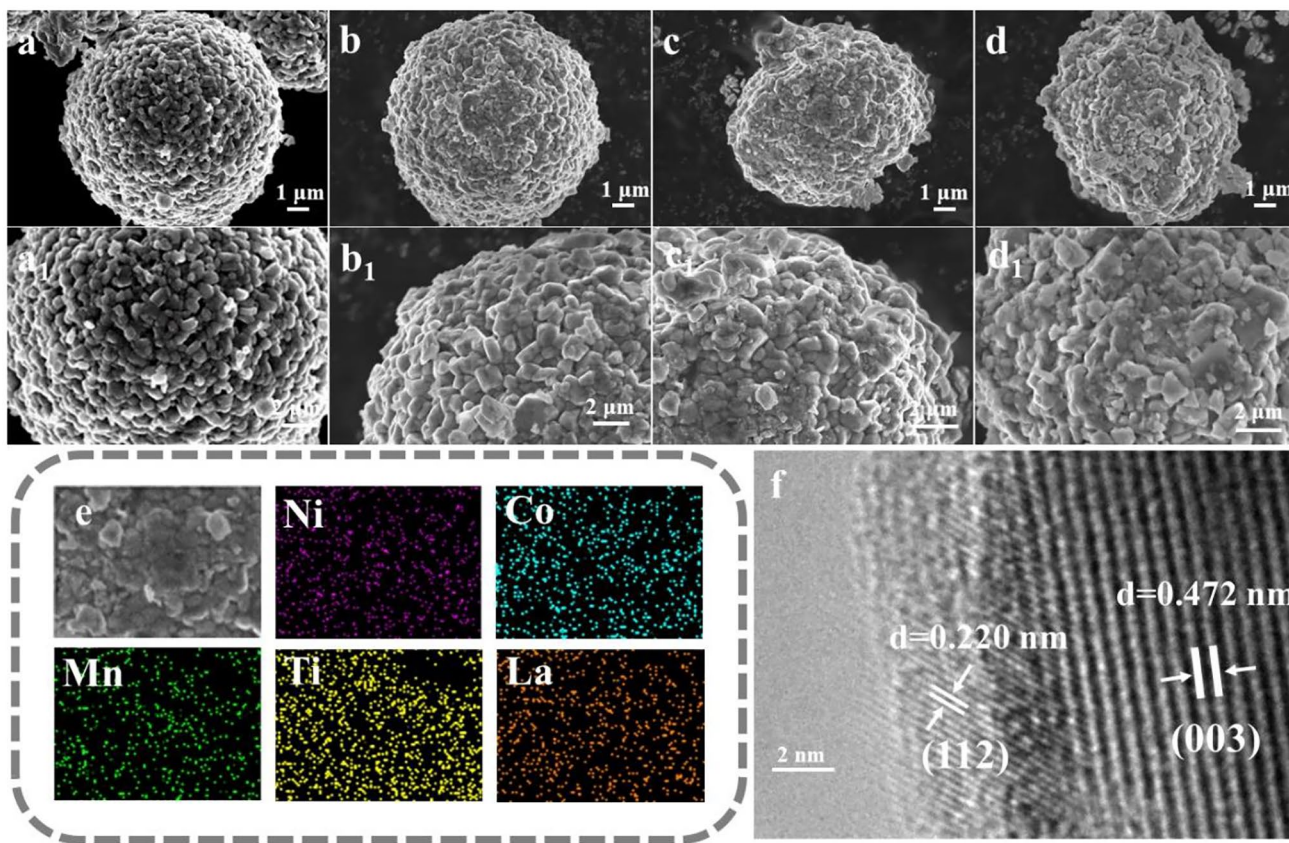


Fig. 3 Scanning electron microscopy images of NCM83-LLTO with different contents of coating **a** 3 wt%, **b** 5 wt%, **c** 7 wt%, **d** 0; **e** EDS image of NCM83-0.05LLTO; **f** TEM image of NCM83-0.05LLTO at high resolution

capacity of the material coated with 5 wt% LLTO has no significant attenuation after high-rate discharge, which indicates that the material has good reversibility. In particular, the discharge-specific capacity of the LLTO-coated NCM83 is 157.8 mAh g⁻¹ at 5 C, which corresponds to a capacity

retention rate of 81.2% at 0.2 C. The significantly improvement in the NCM83-0.05LLTO rate capability is mainly attributed to the high Li⁺ conductivity of the LLTO coating layer, which provides a channel for Li⁺ ion during charging and discharging and facilitates the Li⁺ ion transport.

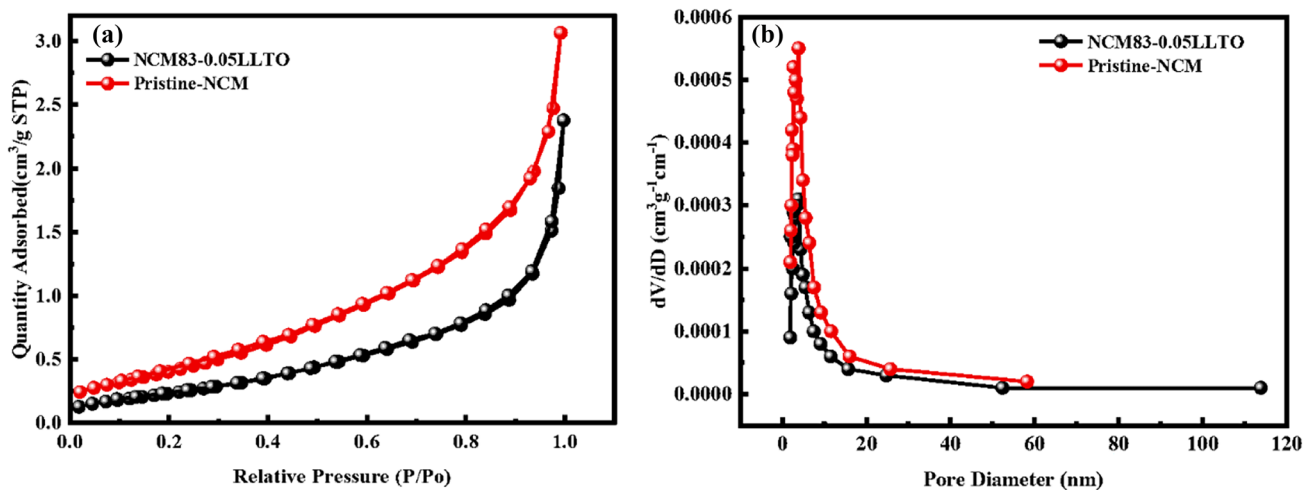


Fig. 4 **a** The N₂ adsorption–desorption isotherm curves, **b** pore size distribution curves of Pristine-NCM and NCM83-0.05LLTO

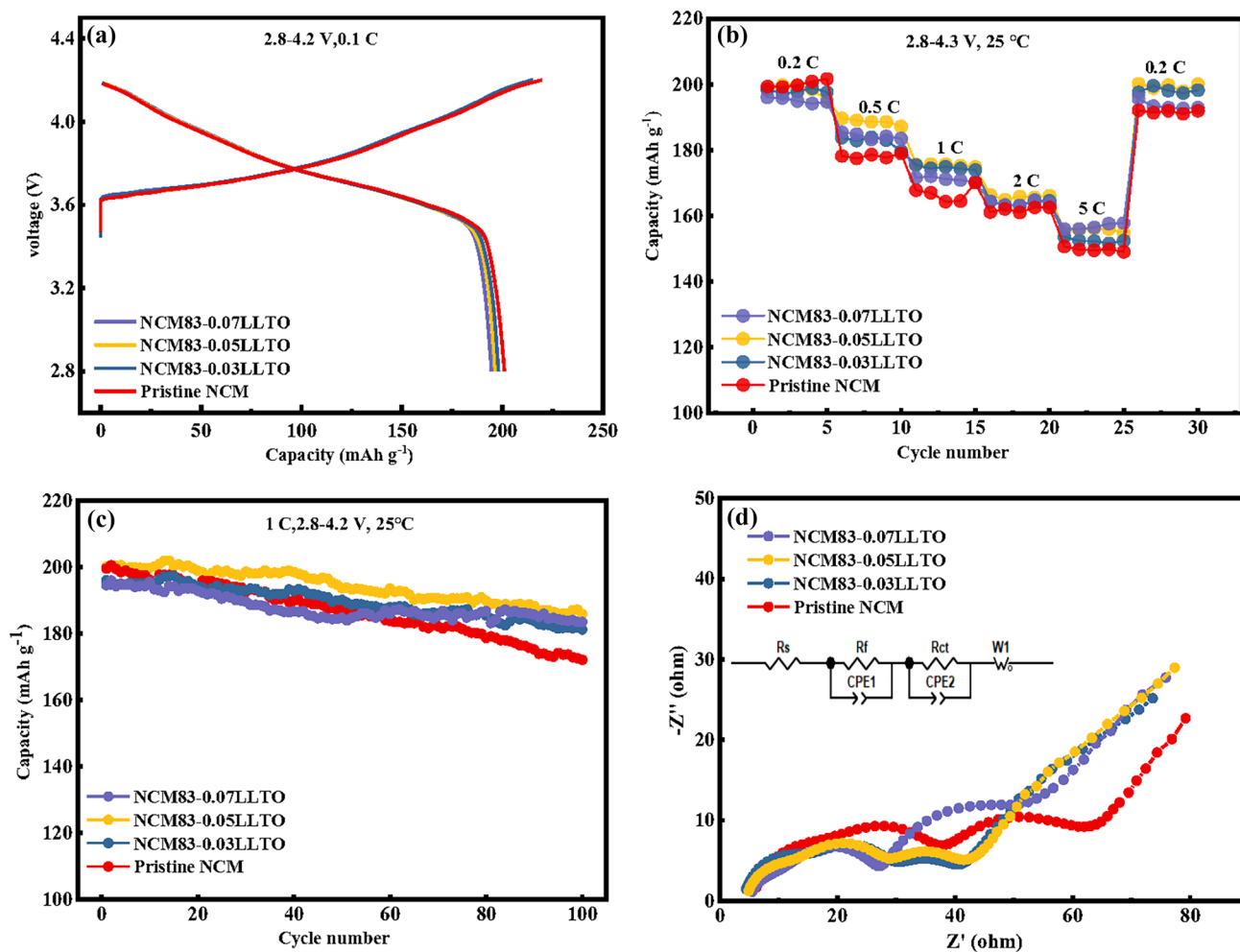


Fig. 5 **a** First charge/discharge curves of NCM83-LLTO with different contents; **b** Rate cycling curves of NCM83-LLTO with different contents; **c** cycling performance curves of NCM83-LLTO with different contents; **d** EIS fitting curves of NCM83-LLTO with different contents.

Figure 5c shows the cycling curves of four samples at 1 C for 100 cycles at room temperature. After 100 cycles, the discharge-specific capacities of Pristine-NCM, NCM83-0.03LLTO, NCM83-0.05LLTO, and NCM83-0.07LLTO are 172.1 mAh g⁻¹, 181.2 mAh g⁻¹, 185.9 mAh g⁻¹, and 183.4 mAh g⁻¹, respectively. The LLTO-coated materials have better cycling performance with capacity retention rates of 92% or more compared with the uncoated samples of 86.23%. The excellent cycle performance is mainly attributed to the fact that the LLTO coating layer inhibits the surface side reactions and enhances the interface stability. After the formation of LLTO coating, the surface gap is reduced, which reduces the erosion of the primary particles by the electrolyte, inhibits the growth of microcracks during cycling, relieves the accumulation of internal stresses, and improves the stable performance of the material structure. The fast-ion conductor can promote ion migration and alleviate the increase in interface impedance during Li⁺ ion

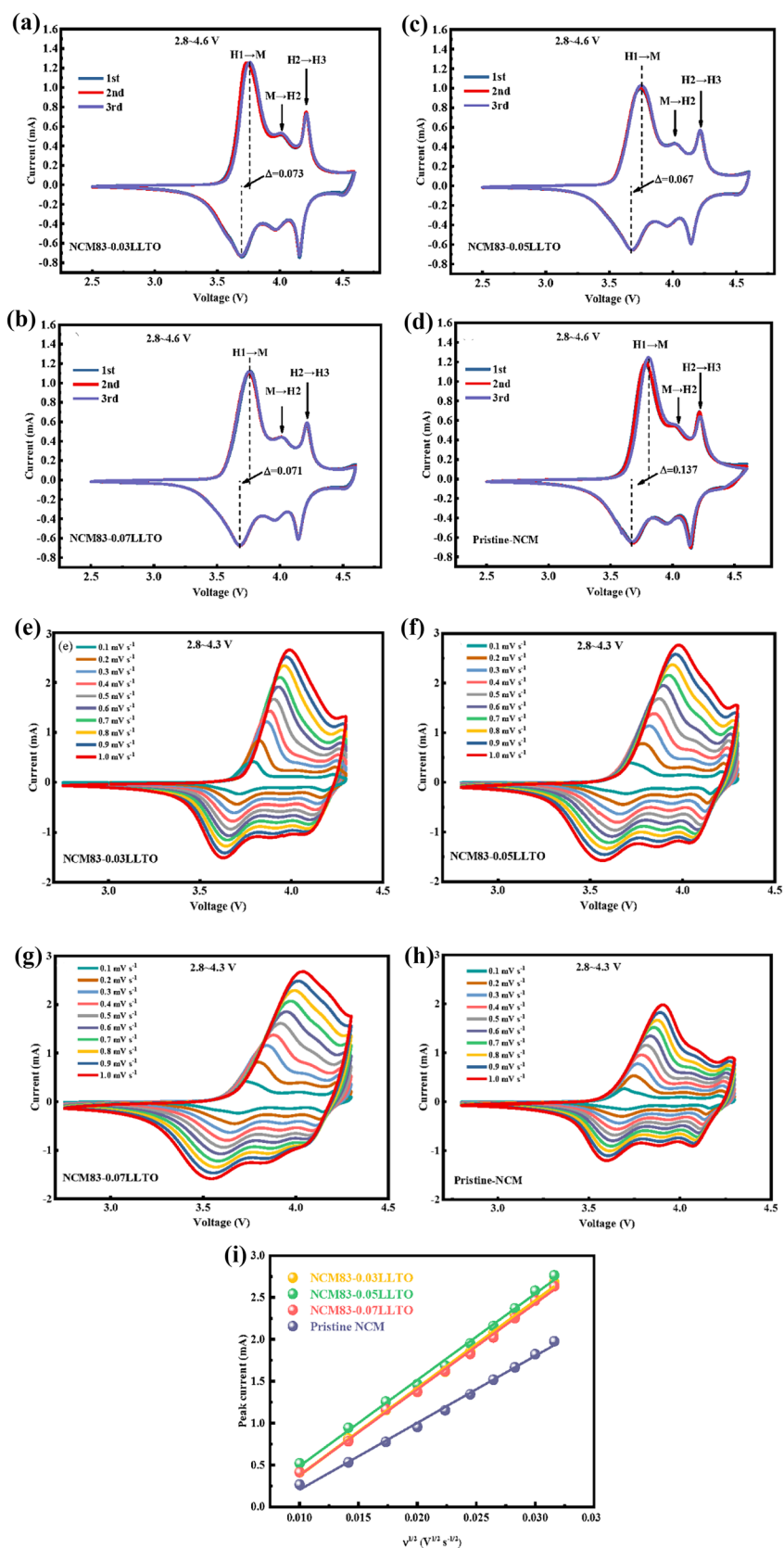
deintercalation, so the process of LLTO coating can effectively improve the cycle performance of NCM.

To better understand the effect of the LLTO coating on the NCM surface, electrochemical impedance spectroscopy is performed on each sample after 5 cycles at 0.1 C. As shown in Fig. 5d, the EIS curve consists of three parts, the first arc represents the semicircle of the high-frequency region of the surface SEI film impedance ($R_{s,f}$), the second arc represents the charge transfer resistance (R_{ct}), and the third part is a

Table 1 Diffusion coefficients of Li⁺ for different samples

Samples	$D_{\text{Li-insertion}}$ (cm ² ·s ⁻¹)
Pristine-NCM	8.757×10^{-12}
NCM83-0.03LLTO	1.127×10^{-11}
NCM83-0.05LLTO	1.143×10^{-11}
NCM83-0.07LLTO	1.123×10^{-11}

Fig. 6 **a, b, c,** and **d** show the Pristine-NCM, NCM83-0.03LLTO, and NCM83-0.05LLTO, respectively. NCM83-0.07LLTO at a scan rate of 0.2 mV s^{-1} for three cycles of voltammetry; **e, f, g,** and **h** are cyclic voltammetry curves at different scan rates; **i** shows a linear fit corresponding to the square root between the peak current and the scan rate



diagonal line representing the Warburg impedance (Z_w). The R_{sf} and R_{ct} of the uncoated sample are 37.35 Ω and 24.68 Ω , respectively, while the LLTO-coated samples exhibit relatively low impedance values, and the R_{sf} and R_{ct} of NCM-0.05 LLTO are 29.15 Ω and 12.36 Ω , respectively. During the electrochemical reaction, lithium residual reactants may accumulate on the interface of the material, causing discontinuous electron/ion transfer, resulting in an increase in the interfacial membrane impedance and charge transfer impedance [44]. The LLTO coating stabilizes the NCM83 surface, mitigates the electrolyte attack on the material and slows down the rate of SEI film formation.

To further investigate the electrochemical kinetics of the cathode materials, cyclic voltammetry tests (CV) are performed on different coating NCM83-LLTO materials. Figure 6a–c, and d are the 3-loop CV curves at a scan rate of 0.2 mV s^{-1} from 2.5 to 4.6 V. The CV curves of the samples with different LLTO coverings contents show the typical characteristics of high Ni materials, that is, three-phase transition processes ($H1 \rightarrow M \rightarrow H2 \rightarrow H3$) [45] occur in the range of 3.6–3.9 V, 3.9–4.0 V, and 4.0–4.3 V, respectively. The ΔE difference is usually used to determine the strength of the polarization and the reversibility of the cycle. The potential difference is calculated to be the largest for Pristine-NCM and the smallest for NCM83-0.05LLTO, with potential differences of 0.137 mV and 0.067 mV, respectively. Phase transformation at the end of charging often causes a sharp contraction of the lattice parameter c , resulting in anisotropic changes in cell volume and local stress accumulation, which eventually leads to the generation of microcracks. The LLTO coating can fill some of the voids between the primary particles to make the material structure more dense, inhibit the formation and growth of microcracks, and mitigate the adverse effects of volume change and stress accumulation during cycling. Therefore, the potential difference of the LLTO-coated material is smaller, and the reversibility is best during the charging and discharging process, which is also consistent with its BET test and cycling test results.

It is obvious that the LLTO coating has a great influence on the electrochemical performance of the NCM83 materials; therefore, the cyclic voltammetry (CV) tests with different scan rates are performed to further investigate the performance of the material, and the results are shown in Fig. 6e–h. Due to the polarization and irreversibility of the material in the redox process, the potential difference between the oxidation and reduction peaks gradually increases with the increase of the scanning speed, which is related to the electrode reaction. The diffusion coefficients of lithium ions in the four samples can be calculated by Eq. (1) [46].

$$i = 2.69 \times 10^5 n^{3/2} A D^{1/2} v^{1/2} C_0 \quad (1)$$

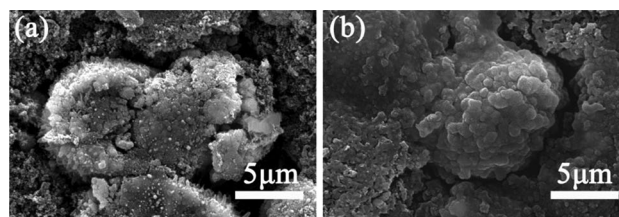


Fig. 7 SEM images after 100 cycles (a) Pristine-NCM, (b) NCM83-0.05LLTO

In which the parameter n represents the electron transfer number of the reactant ($n = 1$ for Li^+), A is the active area of the pole piece, D is the diffusion coefficient of Li^+ , and C_0 is the change in Li^+ concentration corresponding to a specific electrochemical reaction. The peak current (i) varies linearly with the scan rate (v). From Table 1, as expected, the LLTO-coated NCM83 has a higher Li^+ diffusion coefficient, and the LLTO coating with high ionic conductivity provides a channel for Li^+ transport and increases the Li^+ diffusion rate.

After 100 cycles, the battery was disassembled, and the morphology of the positive electrode particles was obtained, as shown in Fig. 7a, b. By comparison, it was found that almost all of the Pristine-NCM material showed cracks, while NCM83-0.05LLTO showed almost no cracks after 100 cycles. This indicates that the modification of LLTO can ensure the structural integrity of Ni-rich cathode materials, thereby improving their cycling performance, which is consistent with the electrochemical cycling performance results.

Conclusions

In summary, the fast-ion conductor LLTO coating with the thickness of 2 nm is constructed on the surface of lithium-ion cathode material $\text{LiNi}_{0.83}\text{Co}_{0.12}\text{Mn}_{0.05}\text{O}_2$ material in situ by a simple sol–gel method, which solves the problem of poor cycling stability caused by the interfacial instability and structural degradation of the cathode material. The LLTO coating can provide a transport channel for Li^+ ion, alleviate the electrolyte erosion of the active material, and significantly improve the Li^+ ion diffusion and structural stability, which makes the material have excellent rate performance and cycle performance. This study provides an effective pathway for rational material surface modification and scalable preparation and can be extended to other cathode materials.

Funding This work was financially supported by the Education Department of Jiangxi Province (No. GJJ160202, no. GJJ190428).

Data availability The data that support the findings of this study are available from the corresponding author upon reasonable request.

References

- Hao H, Cheng X, Liu Z, Zhao F (2017) China's traction battery technology roadmap: targets, impacts and concerns. *Energy Policy* 108:355–358
- Miao Y, Hynan P, Von Jouanne A, Yokochi A (2019) Current Li-ion battery technologies in electric vehicles and opportunities for advancements. *Energies* 12(6):1074
- Li H, Liu W, Yang X, Xiao J, Li Y, Sun L, Ren X, Zhang P, Mi H (2021) Fluoroethylene carbonate-Li-ion enabling composite solid-state electrolyte and lithium metal interface self-healing for dendrite-free lithium deposition. *Chem Eng J* 408:127254
- Li A, Li G, Lu S, Ren Z, Wang J, Zhuo H, Quan W, Zhang G, Han F, Xia Y, Wang J, Zhang Y (2022) Interface stabilization of 1,1,2,2-tetrafluoroethyl-2,2,3,3-tetrafluoropropyl ether to high-voltage Li-rich Mn-based layered cathode materials. *Rare Met* 41(3):822–829
- Zubi G, Dufo-López R, Carvalho M, Pasaoglu G (2018) The lithium-ion battery: state of the art and future perspectives. *Renew Sust Energ Rev* 89:292–308
- Li W, Evan M, Manthiram A (2020) High-nickel layered oxide cathodes for lithium-based automotive batteries. *Nat Energy* 5(1):26–34
- Pender JP, Jha G, Youn DH, Ziegler JM, Andoni I, Choi EJ, Heller A, Dunn BS, Weiss PS, Penner RM, Mullins CB (2020) Electrode degradation in lithium-ion batteries. *ACS Nano* 14(2):1243–1295
- Zhang SS (2020) Problems and their origins of Ni-rich layered oxide cathode materials. *Energy Stor Mater* 24:247–254
- Zhang S, Ma J, Hu Z, Cui G, Chen L (2019) Identifying and addressing critical challenges of high-voltage layered ternary oxide cathode materials. *Chem Mater* 31(16):6033–6065
- Liu L, Li M, Chu L, Jiang B, Lin R, Zhu X, Cao G (2020) Layered ternary metal oxides: performance degradation mechanisms as cathodes, and design strategies for high-performance batteries. *Prog Mater Sci* 111:100655
- Qian H, Ren H, Zhang Y, He X, Li W, Wang J, Hu J, Yang H, Sari HM, Chen Y, Li X (2022) Surface doping vs. bulk doping of cathode materials for lithium-ion batteries: a review. *Electrochem Energy Rev* 5(4):1–32
- Hou P, Yin J, Ding M, Huang J, Xu X (2017) Surface/interfacial structure and chemistry of high-energy nickel-rich layered oxide cathodes: advances and perspectives. *Small* 13(45):1701802
- Kim DH, Song JH, Jung CH, Eum D, Kim B, Hong SH, Kang K (2022) Stepwise dopant selection process for high-nickel layered oxide cathodes. *Adv Energy Mater* 12(18):2200136
- Yin S, Deng W, Chen J, Gao X, Zou G, Hou H, Ji X (2021) Fundamental and solutions of microcrack in Ni-rich layered oxide cathode materials of lithium-ion batteries. *Nano Energy* 83:105854
- Guan P, Zhou L, Yu Z, Sun Y, Liu Y, Wu F, Jiang Y, Chu D (2020) Recent progress of surface coating on cathode materials for high-performance lithium-ion batteries. *J Energy Chem* 43:220–235
- Nisar U, Muralidharan N, Essehli R, Amin R, Belharouak I (2021) Valuation of surface coatings in high-energy density lithium-ion battery cathode materials. *Energy Stor Mater* 38:309–328
- Sun HH, Ryu HH, Kim UH, Weeks JA, Heller A, Sun YK, Mullins CB (2020) Beyond doping and coating: prospective strategies for stable high-capacity layered Ni-rich cathodes. *ACS Energy Lett* 5(4):1136–1146
- Qiu L, Zhang M, Song Y, Xiao Y, Wu Z, Xiang W, Liu Y, Wang G, Sun Y, Zhang J, Zhang B (2021) Recent advance in structure regulation of high-capacity Ni-rich layered oxide cathodes. *Eco-Mat* 3(5):e12141
- Chen Z, Zhang W, Yang Z (2019) A review on cathode materials for advanced lithium ion batteries: microstructure designs and performance regulations. *Nanotechnology* 31(1):012001
- Liu HH, Zhang J, Lou YW, Yang CZ, Xie XH, Xia BJ (2012) Structure evolution and electrochemical performance of Al₂O₃-coated LiNi_{0.4}Co_{0.2}Mn_{0.4}O₂ during charge-discharge cycling. *Chem Res Chin Univ* 28(4):686–690
- Dong M, Wang Z, Li H, Guo H, Li X, Shih K, Wang J (2017) Metallurgy inspired formation of homogeneous Al₂O₃ coating layer to improve the electrochemical properties of LiNi_{0.8}Co_{0.1}Mn_{0.1}O₂ cathode material. *ACS Sustain Chem Eng* 5(11):10199–10205
- Ma F, Wu Y, Wei G, Qiu S, Qu J (2019) Enhanced electrochemical performance of LiNi_{0.8}Co_{0.1}Mn_{0.1}O₂ cathode via wet-chemical coating of MgO. *J Solid State Electrochem* 23(7):2213–2224
- Laskar MR, Jackson DH, Xu S, Hamers RJ, Morgan D, Kuech TF (2017) Atomic layer deposited MgO: a lower overpotential coating for Li[Ni_{0.5}Mn_{0.3}Co_{0.2}]O₂ cathode. *ACS Appl Mater Interfaces* 9(12):11231–11239
- Zha G, Luo Y, Hu N, Ouyang C, Hou H (2020) Surface modification of the LiNi_{0.8}Co_{0.1}Mn_{0.1}O₂ cathode material by coating with FePO₄ with a yolk-shell structure for improved electrochemical performance. *ACS Appl Mater Interfaces* 12(32):36046–36053
- Xia S, Li F, Chen F, Guo H (2018) Preparation of FePO₄ by liquid-phase method and modification on the surface of LiNi_{0.80}Co_{0.15}Al_{0.05}O₂ cathode material. *J Alloys Compd* 731:428–436
- Lee DJ, Scrosati B, Sun YK (2011) Ni₃(PO₄)₂-coated Li[Ni_{0.8}Co_{0.15}Al_{0.05}]O₂ lithium battery electrode with improved cycling performance at 55°C. *J Power Sources* 196(18):7742–7746
- Cui Y, Xu S (2015) High tap density of Ni₃(PO₄)₂ coated LiNi_{1/3}Co_{1/3}Mn_{1/3}O₂ with enhanced cycling performance at high cut-off voltage. *Chin J Chem Eng* 23(1):315–320
- Dai S, Yan G, Wang L, Luo L, Li Y, Yang Y, Liu H, Liu Y, Yuan M (2019) Enhanced electrochemical performance and thermal properties of Ni-rich LiNi_{0.8}Co_{0.1}Mn_{0.1}O₂ cathode material via CaF₂ coating. *J Electroanal Chem* 847:113197
- Shi SJ, Tu JP, Mai YJ, Zhang YQ, Tang YY, Wang XL (2012) Structure and electrochemical performance of CaF₂ coated LiNi_{1/3}Co_{1/3}Mn_{1/3}O₂ cathode material for Li-ion batteries. *Electrochim Acta* 83:105–112
- Shapira A, Tiurin O, Solomatin N, Auinat M, Meitav A, Ein-Eli Y (2018) Robust AlF₃ atomic layer deposition protective coating on LiMn_{1.5}Ni_{0.5}O₄ particles: an advanced Li-ion battery cathode material powder. *ACS Appl Energy Mater* 1(12):6809–6823
- Hu G, Qi X, Hu K, Lai X, Zhang X, Du K, Peng Z, Cao Y (2018) A facile cathode design with a LiNi_{0.6}Co_{0.2}Mn_{0.2}O₂ core and an AlF₃-activated Li_{1.2}Ni_{0.2}Mn_{0.6}O₂ shell for Li-ion batteries. *Electrochim Acta* 265:391–399
- Yan P, Zheng J, Liu J, Wang B, Cheng X, Zhang Y, Sun X, Wang C, Zhang JG (2018) Tailoring grain boundary structures and chemistry of Ni-rich layered cathodes for enhanced cycle stability of lithium-ion batteries. *Nat energy* 3(7):600–605
- Xiao Z, Chi Z, Song L, Cao Z, Li A (2020) LiTa₂PO₈ coated nickel-rich cathode material for improved electrochemical performance at high voltage. *Ceram Int* 46(6):8328–8333
- Fan Z, Xiang J, Yu Q, Wu X, Li M, Wang X, Xia X, Tu J (2021) High performance single-crystal Ni-rich cathode modification via crystalline LLTO nanocoating for all-solid-state lithium batteries. *ACS Appl Mater Interfaces* 14(1):726–735
- Liu S, Zhang C, Su Q, Li L, Su J, Huang T, Chen Y, Yu A (2017) Enhancing electrochemical performance of LiNi_{0.6}Co_{0.2}Mn_{0.2}O₂ by lithium-ion conductor surface modification. *Electrochim Acta* 224:171–177
- Cho DH, Jo CH, Cho W, Kim YJ, Yashiro H, Sun YK, Myung ST (2014) Effect of residual lithium compounds on layer Ni-rich Li[Ni_{0.7}Mn_{0.3}]O₂. *J Electrochem Soc* 161(6):A920–A926

37. Zhang MJ, Hu X, Li M, Duan Y, Yang L, Yin C, Ge M, Xiao X, Lee WK, Ko JY, Amine K (2019) Cooling induced surface reconstruction during synthesis of high-Ni layered oxides. *Adv Energy Mater* 9(43):1–10
38. Martinez AC, Grugeon S, Cailleu D, Courty M, Tran-Van P, Delobel B, Laruelle S (2020) High reactivity of the nickel-rich $\text{LiNi}_{1-x-y}\text{Mn}_x\text{Co}_y\text{O}_2$ layered materials surface towards $\text{H}_2\text{O}/\text{CO}_2$ atmosphere and LiPF_6 -based electrolyte. *J Power Sources* 468:228204
39. Seong WM, Cho KH, Park JW, Park H, Eum D, Lee MH, Kim IS, Lim J, Kang K (2020) Controlling residual lithium in high-nickel (> 90%) lithium layered oxides for cathodes in lithium-ion batteries. *Angew Chem Int Ed* 59(42):18662–18669
40. Wang X, Ding YL, Deng YP, Chen Z (2020) Ni-Rich/Co-poor layered cathode for automotive Li^- ion batteries: promises and challenges. *Adv Energy Mater* 10(12):1903864
41. Wang R, Li Z, Yang Z, Zhang M, Zhang D, Yan Y (2021) Synergistic effect of Ce^{4+} modification on the electrochemical performance of $\text{LiNi}_{0.6}\text{Co}_{0.2}\text{Mn}_{0.2}\text{O}_2$ cathode materials at high cut-off voltage. *Ceram Int* 47(1):1268–1276
42. Mei A, Jiang QH, Lin YH, Nan CW (2009) Lithium lanthanum titanium oxide solid-state electrolyte by spark plasma sintering. *J Alloys Compd* 486(1–2):871–875
43. Sun HH, Manthiram A (2017) Impact of microcrack generation and surface degradation on a nickel-rich layered $\text{Li}[\text{Ni}_{0.9}\text{Co}_{0.05}\text{Mn}_{0.05}]\text{O}_2$ cathode for lithium-ion batteries. *Chem Mater* 29(19):8486–8493
44. Chen A, Wang K, Li J, Mao Q, Xiao Z, Zhu D, Wang G, Liao P, He J, You Y, Xia Y (2020) The formation, detriment and solution of residual lithium compounds on Ni-rich layered oxides in lithium-ion batteries. *Front Energy Res* 8:593009
45. Zheng S, Hong C, Guan X, Xiang Y, Liu X, Xu GL, Liu R, Zhong G, Zheng F, Li Y, Zhang X (2019) Correlation between long range and local structural changes in Ni-rich layered materials during charge and discharge process. *J Power Sources* 412:336–343
46. Tang Z, Wang S, Liao J, Wang S, He X, Pan B, He H, Chen C (2019) Facilitating lithium-ion diffusion in layered cathode materials by introducing $\text{Li}^+/\text{Ni}^{2+}$ antisite defects for high-rate Li-ion batteries. *Research* 2019:2198906

Publisher's Note Springer Nature remains neutral with regard to jurisdictional claims in published maps and institutional affiliations.

Springer Nature or its licensor (e.g. a society or other partner) holds exclusive rights to this article under a publishing agreement with the author(s) or other rightsholder(s); author self-archiving of the accepted manuscript version of this article is solely governed by the terms of such publishing agreement and applicable law.